https://doi.org/10.52676/1729-7885-2023-4-91-97
УДК 538.94

AB-INITIO CALCULATIONS OF RHOMBOHEDRAL $BaTiO_3$ (111) SURFACE COMBINED WITH GRAPHENE FILMS

B. M. Satanova[1*], G. A. Kaptagay[2], A. P. Zharkymbekova[1], F. U. Abuova[1], A. U. Abuova[1], R. N. Assylbayev[3], N. O. Koylyk[2], K. T. Tugelbayeva[2]

[1] L. N. Gumilyov Eurasian National University, Astana, Kazakhstan
[2] Kazakh National Women's teacher training University, Almaty, Kazakhstan
[3] Pavlodar Pedagogical University named after A. Margulan, Pavlodar, Kazakhstan

** E-mail for contacts: clever_s.balzhan@mail.ru*

Thin films of ABO_3 perovskite ferroelectrics are important for many industrial applications, i.e., high-capacity memory cells, catalysis, optical waveguides, and integrated optics. The use of $BaTiO_3$ for these industries and products is due to the variety of its surface structure and, accordingly, its electronic and chemical properties. Calculations of the surface characteristics of $BaTiO_3$ from the first principles are useful for understanding processes that play a crucial role, such as surface reaction chemistry, surface phenomena, and adsorption surfaces. This study examined theoretical calculations related to the relaxed atomic structures of the surface of $BaTiO_3$ (111).

Keywords: *heterostructures, two-dimensional materials, small-dimensional structure, transition metal oxides, Hartree-Fock hybrid correlation function.*

INTRODUCTION

$BaTiO_3$ is a popular classic electrician with a wide range of applications, from dielectric capacitors to non-linear optical devices. $BaTiO_3$ cubic-structured lattice is paraelectric at high temperatures [1].

The effect of deformation on phase transitions and domain structures in thin $BaTiO_3$ films is mainly determined by elastic constants and electrostriction coefficients [2–3].

At temperatures from 0 °C to 120 °C, the structure enters the tetragonal phase (*P4mm* spatial group), where the Ti atom leaves the center along the Ti-O bond, polarized along [111], and has a value of 26 μl/cm^2. The initial cubic symmetry is as follows: there is an increase in the distorted lattice parameter, and the coordinates at the OII position are 1.011.5. The displacement for atoms Ba2+ and Ti4+ along the c axis will have the values +0.06, +0.12, and −0.03 Å, respectively [4].

When the temperature drops below 0 °C, the orthorhombic phase (spatial group C_2 *mm*) is stable. It is also a self-polarized ferroelectric parallel to the direction of the pseudocube edge (111). At −90 °C, a third phase transition occurs, and the symmetry of the lattice changes rhombohedral (spatial group *Rm3*): a = b = c and α = 89.87°. The electric polarity axis lies in one of the diagonal directions of the pseudocube (111).

In low-temperature ferroelectric phases, self-polarization has ferroelectric, dielectric, piezoelectric, pyroelectric, electro-optical, and nonlinear optical properties [5–6]. Given the transition temperature, the transition from the cubic phase to the tetragonal phase is of particular interest, and a corresponding comparison with cubic perovskites shows that the phase transition behavior in $BaTiO_3$ is not universal but must depend on the details of the chemistry and structural thermodynamics of that compound [9, 10].

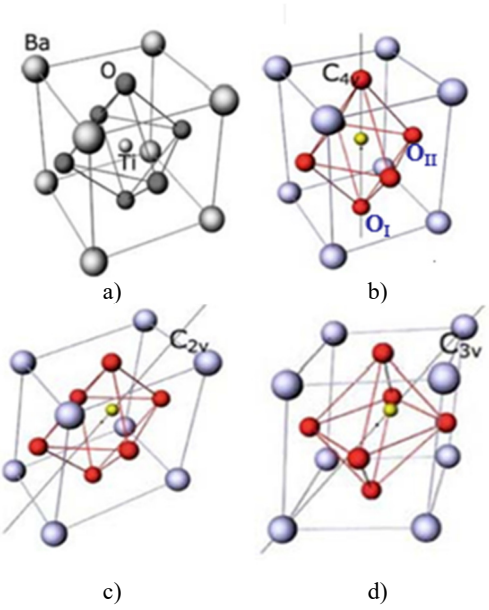

Figure 1. Phase transition of $BaTiO_3$: a) cubic phase, b) tetragonal phase, c) orthorhombic phase, d) rhombohedral phase

Given this technological importance, it is not surprising that the surface of $BaTiO_3$ (111) has theoretically been widely studied using ab initio methods and the shell model [3–9]. Unlike the widely studied $BaTiO_3$ (111) surfaces, only a small part of the work is devoted to calculating the atomic and electronic structure of the $BaTiO_3$ (111) surface [11]. For example, Eglitis and Vanderbilt [12] recently conducted a study of $BaTiO_3$ (111) surfaces using the Hartree-Fock hybrid correlation function (HF) and density functionality theory (DFT), in which the exchange-correlation function HF is mixed with the three-parameter exchange DPF and combined with the non-local correlation function Purdue and Wang (B3pw) [13].

There are no data on experimental studies related to $BaTiO_3$ (111), but there are several experimental studies for surfaces related to $SrTiO_3$ (111). Tanaka and Kawai [10] got clean surfaces on the recovered $SrTiO_3$(111) crystals and used high-energy reflective diffraction to look at them through a scanning tunneling microscope. They observed two different surface structures, one with the SRO crustal layer obtained by annealing at 1180 °C and the Ti outer layer obtained by annealing at 1220 °C [14, 15].

As for the theory, [16], based on the results obtained by the Hartree-Fock full-energy semi-empirical method, (111) and (111) discussed the effect of polarity on the $SrTiO_3$ surfaces. For these areas, they consider some prototypical (1,1) configurations that differ in surface composition and the coordination number of surface atoms. They believe that the compensation of these polar directions is mainly achieved by the abnormal filling of surface states, which must be determined by surface spectroscopy [17].

METHOD FOR SURFACE CALCULATIONS

Calculations were made based on the first principles within the framework of the DFT. Unlike the flat wave codes used in many previous studies, Gaussian-type localized BSS is used. In the calculations of Eglitis and his colleagues, BSS was developed for $SrTiO_3$, $BaTiO_3$, and $PbTiO_3$. Many calculations for O atoms used a new BS, which differs in the addition of d orbitals that polarize in O ions. Crystalline BS is generally considered transportable, and therefore, since it is defined for some chemical component, it can be successfully used in calculations for various chemicals such as Srf_2, BaF_2, and CaF_2. Most of the calculations in this review were performed using the b3pw hybrid exchange-correlation functor, including non-local focal precision exchange, local density approximation (LDA), and Becke gradient-adjusted exchange functor, combined with Purdue and Wang's non-local correlation potential [18]. For many studies of the ABO_3 perovskite surface, b3pw was chosen as a hybrid functional because it provides excellent results for the $SrTiO_3$, $BaTiO_3$, and $PbTiO_3$ constant volume lattice and volume module [19].

The inverse space integration was accomplished by sampling the Brilluen area, in most cases using the 8×8×8 Monkhorst–Pack grid, which provides a balanced sum in the forward and reverse spaces. To achieve high accuracy, a sufficiently large tolerance of 7, 8, 7, 7, and 14 was selected for the parameters of dimensionless Coulomb penetration, exchange, first false overlap, and second false overlap, respectively.

SURFACE ENERGY OF ABO_3 PEROVSKITE

Consequently, the $E_{cl}(BaO_3 + Ti)$ cleavage energy is the same for both terminations. The cleavage energy of the complementary $BaTiO_3$ surface $E_{cl}(BaO_3 + Ti)$ can be obtained via the following equation:

$$E_{cl}\left(\mathrm{BaO_3}+\mathrm{Ti}\right)=\frac{1}{4}\left[E_{slab}^{unrel}\left(\mathrm{BaO_3}\right)+E_{slab}^{unrel}\left(\mathrm{Ti}\right)-nE_{bulk}\right], \quad (1)$$

where $E_{slab}^{unrel}\left(\mathrm{BaO_3}\right)$ is the total energy of unrelaxed BaO_3 terminated $BaTiO_3$ (111) surface. $E_{slab}^{unrel}\left(\mathrm{Ti}\right)$ is the total energy of unrelaxed Ti-terminated $BaTiO_3$ (111) surface. E_{bulk} is the bulk energy per formula unit containing 5 atoms in the rhombohedral $BaTiO_3$ structure. nE_{bulk} energy of the corresponding number of $BaTiO_3$ units in the bulk. Factor ¼ means that totally four surfaces are created upon the crystal cleavage. When both sides of the slab are allowed to relax, the relaxation energies for each of the surfaces can be obtained from the equation:

$$E_{rel}\left(\gamma\right)=\frac{1}{2}\left[E_{slab}^{rel}\left(\gamma\right)-E_{slab}^{unrel}\left(\gamma\right)\right], \quad (2)$$

where γ = Ti or BaO_3 specifies the actual $BaTiO_3$ (111) surface. $E_{slab}^{rel}\left(\gamma\right)$ is the Ti or BaO_3-terminated $BaTiO_3$ (111) slab energy after relaxation. $E_{slab}^{unrel}\left(\gamma\right)$ is the Ti or BaO_3-terminated $BaTiO_3$ (111) slab total energy without the geometry relaxation. Factor ½ means that two surfaces are created upon the crystal cleavage. Finally, the $BatiO_3$ (111) surface energy is a sum of the cleavage and relaxation energies:

$$E_{surf}\left(\gamma\right)=E_{cl}\left(\mathrm{BaO_3}+Ti\right)+E_{rel}\left(\gamma\right). \quad (3)$$

One of these slabs is terminated by Ti planes (so-called Ti-terminated $BaTiO_3$ (111) surface) and consists of a supercell containing 124 atoms (Ti-BaO_3-Ti–BaO_3–Ti–BaO_3–Ti–BaO_3–Ti). The second slab is terminated by BaO_3 planes (so-called BaO_3-terminated $BaTiO_3$ (111) surface) and consists of a supercell containing 136 atoms (BaO_3–Ti–BaO_3–Ti–BaO_3–Ti–BaO_3) (see Figure 3). As it is known from previous computational studies dealing with polar $SrTiO_3$, $BaTiO_3$, $CaTiO_3$, $BaZrO_3$, and $SrZrO_3$ (111) surfaces a huge electron redistribution takes place for such terminations in order to cancel the polarity, but the Ti or BaO_3-terminated $BaTiO_3$ (111) surface keeps its insulating character, and therefore such calculations are feasible. Their calculation results demonstrated that charge neutralization and polarity compensation could be achieved by charge redistributions of surface atoms. BaO_3 and Ti-crystallographic planes have different charges. As a result, when considering an asymmetric, stoichiometric plate in which one side is terminated by the Ti-terminated surface, an uncompensated dipole moment arises, giving a total charge $q_{total} = 2.36$. Due to the periodic boundary conditions used, a lattice of artificial dipole moments effectively arises, the interaction between which contributes to the total energy of the system. Excluding this contribution is a difficult task. Therefore, we consider a non-stoichiometric Ti-terminated surface to have a compensated dipole moment. On the other hand, a BaO_3-crystallographic plane-compensated dipole moment arises. Next, the $BaTiO_3$ cleavage and surface

energies were calculated. It is obvious that $BaTiO_3$ perovskite Ti and BaO_3-terminated (111) surfaces are mutually complementary. Surfaces with both terminations arise simultaneously under the cleavage of the crystal, and therefore the relevant cleavage energy is distributed equally between the created surfaces.

RESULTS

Initially, we performed the first-principle calculations of rhombohedral symmetry BTO bulk structure. In Table 1, we compare BTO rhombohedral phase properties obtained using the different functional. Calculated values are also compared with existing experimental and theoretical dates. Theoretical bulk lattice constants and other characteristics are corresponds to theoretical and experimental values. As it is seen from Table 1, use of the hybrid PBE functional generally allows predicting the considered rhombohedral BTO properties consistent to experimental dates taken with various PBE_0, LDA functionals. Shown that basis set change does not affect the results considerably. Especially, the superior agreement between PBE and experimental results can be seen for lattice constant a, axial angle α, fractional displacements z_{Ti}, x_o, z_o (respect to the ideal cubic location) of Ti, O atoms. We know only two theoretical works [21, 22] where three BTO ferroelectric phases have been treated by the same DFT method. Reproduced rhombohedral phase bulk band gap 2,5 eV that in good agreement with results of other theoretical works. However, in these two works mainly the structural properties of the ferroelectric phases have been considered.

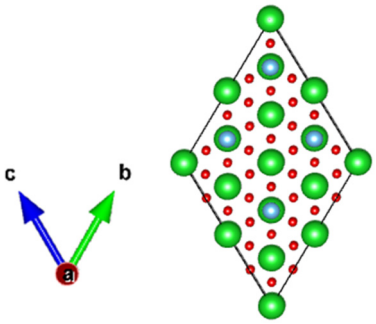

color coding: Ba – green; Ti – blue; O – red

Figure 2. Top view of the (111) rhombohedral $BaTiO_3$

We modeled the $BaTiO_3$ (111) surfaces using symmetric (with respect to the mirror plane) slabs made up of 13 layers of BaO_3 and Ti that alternated with each other. One of these slabs had a supercell with 20 atoms and BaO_3 planes terminating it for the $BaTiO_3$ crystal. The second slab had a supercell with 20 atoms and Ti planes terminating it. These slabs are both stoichiometric, with unit cell formulas of $Ba_4Ti_4O_{12}$.

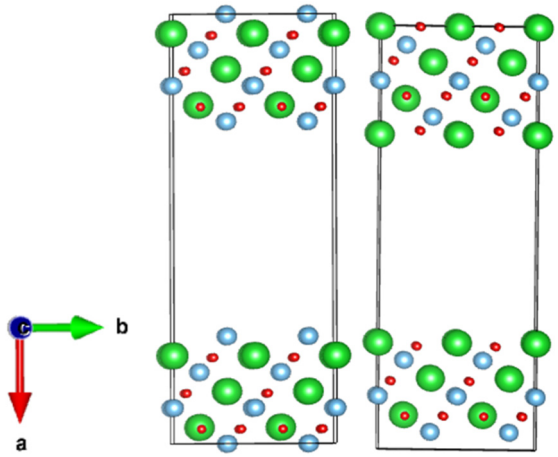

a) b)

Figure 3. Side view of the BaO_3 (a) and Ti (b) terminations of (111) $BaTiO_3$ surface

For this reason, a simple cut creates polar surfaces with BaO_3 ends and Ti ends (111), with nominal surface charges of −2e and +2e per surface cell, this way. If uncompensated, the surface charge would lead to infinite electrostatic cleavage energy. In reality, the polar surfaces would probably become metallic in order to remain neutral, but in view of the large electronic gaps in the perovskites, such metallic surfaces would presumably be unfavorable. Thus, we may expect rather generally that such polar crystal terminations are relatively unstable in this class of materials.

As a next step, the perovskite (111) surfaces were layered with graphene atoms, as shown in Figure 4.

Table 1. Calculated bulk properties of rhombohedral phase of $BaTiO_3$

Parameters*	This work	Other theoretical works					Experiment
		[20][a)]	[20][b)]	[20][c)]	[21][a)]	[22][c)]	[20]
Cell							
a (Å)	4.074	4.073	4.029	3.966	4.073	4.001	4.004
α (deg)	89.754	89.710	89.727	89.958	89.74	89.87	89.8
z_{Ti}	−0.0070	−0.0150	−0.0151	−0.0080	−0.0150	−0.011	−0.01128
x_o	0.0116	0.0143	0.0129	0.0069	0.0141	0.0133	0.0109
z_o	0.0071	0.0249	0.0242	0.0109	0.0245	0.0192	0.0193
Band gap, E_{gap}(eV)	2.5	2.7	4.9	2.2	—	2.3	—
Total energy, ΔE_0 (eV)	−0.005	−0.061	−0.061	−0.005	−0.060	−0.040	—

Notes: * Lattice parameter, a; Axial angel of lattice, α; Fractional displacements z_{Ti}, x_o, z_o of atoms (Ti, O) are given in respect to the ideal cubic location; Total energy, ΔE_0, is calculated relative to the cubic phase; [a)] PBE, [b)] PBE0, [c)] LDA.

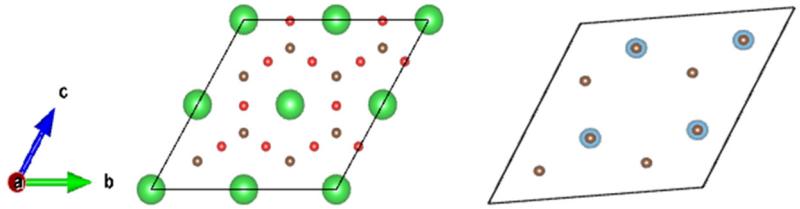

Figure 4. Top view of the BaO_3 (a) and Ti-terminated (b) graphene modified (111) surfaces of $BaTiO_3$

After optimization the Ti-terminated (b) graphene modified (111) surface was unstable, in contrast on the BaO_3-terminated surface shows good adsorption (Figure 5).

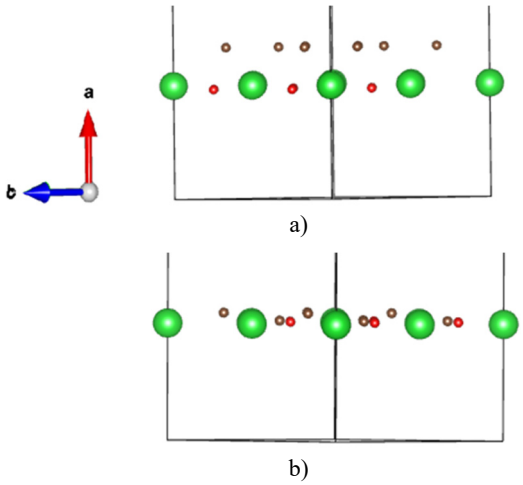

Figure 5. Side view of the initial (a) and optimized (b) BaO_3-terminated graphene modified surface

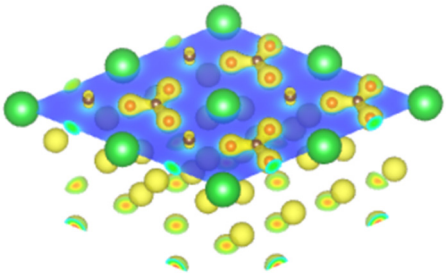

Figure 6. Charge distribution on BaO_3-terminated graphene modified surface

This study used the GGA method to find the theoretical bulk lattice constants for rhombohedral $BaTiO_3$ (4.07 Å). The theoretical value of the lattice constant 1,6% is larger than the corresponding experimental value of 4.00 Å. implemented the Bader method to analyze charge redistribution.

BaO_3 and Ti-crystallographic planes have different charges. As a result, when considering an asymmetric, stoichiometric plate in which one side is terminated by the Ti-terminated surface, an uncompensated dipole moment arises, giving a total charge $q_{total} = 2.36$. Due to the periodic boundary conditions used, a lattice of artificial dipole moments effectively arises, the interaction between which contributes to the total energy of the system. Excluding this contribution is a difficult task. Therefore, we consider a non-stoichiometric Ti-terminated surface to have a non-compensated dipole moment. On the other hand, a BaO_3-crystallographic plane-compensated dipole moment arises. Table 2 shows two types of terminations.

Table 2. Sequence of atomic layers in model plates of (a) BaO_3- and (b) Ti-terminated surfaces

a) BaO_3-terminated $BaTiO_3$ (111)	b) Ti-terminated $BaTiO_3$ (111)
BaO_3	Ti
Ti	BaO_3
BaO_3	Ti
Ti	BaO_3
BaO_3	Ti
Ti	BaO_3
BaO_3	Ti

The calculated surface cleavage energy is 8.73 eV. Surface relaxation energy for BaO_3-terminated $BaTiO_3$ (111) surface (−0.87 eV) is more than two times larger than the corresponding surface relaxation energy for Ti-terminated $BaTiO_3$ (111) surface (−0.30 eV). Consequently, the calculated surface energy for BaO_3-terminated surfaces is equal to 7.86 eV and is 8.44 eV for Ti-terminated surfaces. Calculated cleavage, relaxation, and surface energies for two terminated (111) surfaces of $BaTiO_3$ are in good agreement with other theoretical works.

To describe the electron density distribution, we found the topological (Bader) charges on the atoms in the top and bottom atomic layers and compared them to the values for the bulk crystal $BaTiO_3$. The calculation results are shown in Table 3.

Table 3. Effective topological charge on atoms for a 7-layer plate model with a BaO_3 surface atomic layer compared with a similar value for volumetric $BaTiO_3$

Plane	Atoms	Bulk	Surface	Increment
1	Ba	1.91	1.58	−0.33
	O	−1.29	−1.33	0.04
2	Ti	1.96	2.07	0.11
3	Ba	1.91	1.58	−0.33
	O	−1.29	−1.31	0.02
4	Ti	1.96	2.08	0.12
5	Ba	1.91	1.65	−0.26
	O	−1.29	−1.13	0.16
6	Ti	1.96	2.09	0.13
7	Ba	1.91	1.64	−0.27
	O	−1.29	−1.14	0.15

In a $BaTiO_3$ bulk crystal, the values of the topological charge on the ions are significantly less than the nominal charge due to their valences: Ba3+, Ti3+, and O_2. This fact is due to the fact that part of the electron density is located between ions and gives a covalent contribution to the chemical bond between Ba and O ions. BaO_3- and Ti-terminated surfaces exhibit different behavior: the values of the effective charges on the Ti layers bordering the vacuum remain very close to the values in the bulk sample, while the effective charges on the Ti surface layers decrease significantly compared to the same value for the bulk sample. The effective charges of the remaining atoms inside the plate are close to the corresponding values in volumetric $BaTiO_3$.

Calculated charge redistribution of $BaTiO_3$ Ti-terminated graphene layered surface. The charge density difference of $BaTiO_3$ Ti-terminated graphene-layered surfaces is presented.

In the diagram of the density of state of the BaO_3-terminated $BaTiO_3$ (111) surface (see Figure 7) it is clear that the reproduced band gap is 1.9 eV. In the work for cubic phase BTO (111), the theoretical band gap equals 3.6 eV, while the experimentally defined value equals 3.3 eV. Thus, the disperance of the value of the band gap is explained in our research from experiential and theoretical values explained with the difference of phases of BTO.

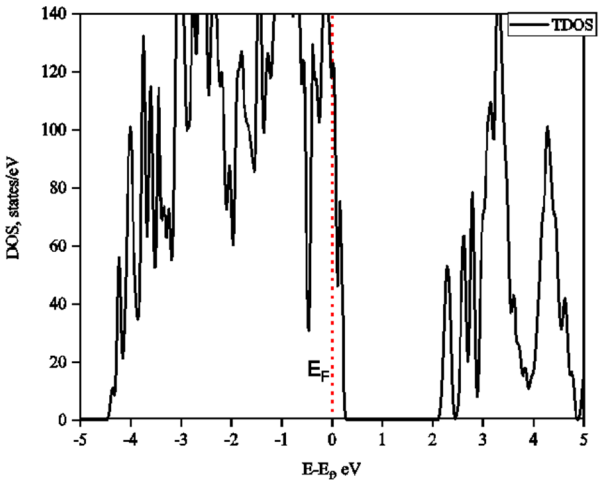

Figure 7. Total density of states for a BaO_3-terminated $BaTiO_3$ (111) surface. The Fermi level is taken equal to zero 2.2, 2.4 and 2.7 eV

As seen from Figure 7, the band gap of the BaO_3-terminated $BaTiO_3$ (111) surface amounts to 1,9 eV, which is close to values of 2.2, 2.4 and 2.7 eV. And plotted the total density of states for a BaO_3-terminated $BaTiO_3$ (111) surface (Figure 8).

According to the performed calculation results for BaO_3-terminated $BaTiO_3$ (111) surfaces relaxation small ranging from 0.02 till 0.24 (see Table 4). BaO_3-terminated and Ti-terminated $BaTiO_3$ (111) surfaces displacements similar, upper layer Ba atoms relax inwards and O atoms relax outwards. Surface upper layer Ba atom relaxes inward by 0.16%, but O atom moves outward by 0.17%. The second layer Ti atom for both termination relaxes inward by 0.1% and 0,24% for unipolar and polar terminations, respectively. Next layer ions of surfaces move like as upper layer Next inner layer Ba atom relaxes outward by 0.09%, but O atom preserve initial state. Ti-terminated surface inner layer Ti ion moves inward very small value 0,18% and 0,02%, respectively. These results are in good agreement with similar data from the work [24].

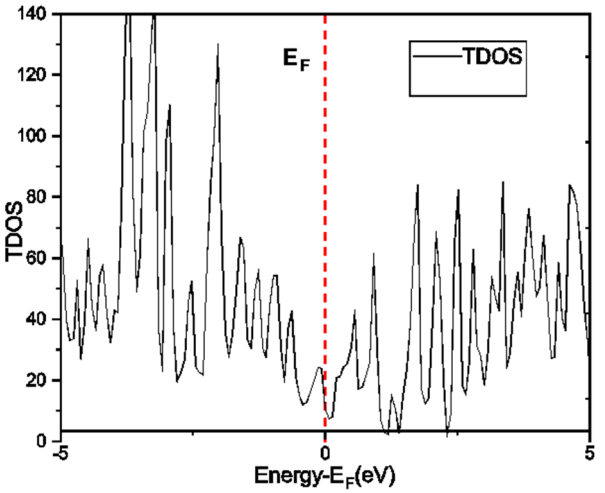

Figure 8. Total density of states for a graphene layered BaO_3-terminated $BaTiO_3$ (111) surface. The Fermi level is taken equal to zero 2.2, 2.4 and 2.7 eV

Table 4. Calculated relaxation of BaO_3 and Ti-terminated $BaTiO_3$ (111) surfaces upper three layer atoms (as a percentage of the bulk crystal lattice constant a = 4.074 Å). Positive (negative) values refer to displacements in the direction outwards (inwards) of the surface

Layer	Ion	Displ. (Δz) BaO_3-term.	Displ. (Δz) Polar BaO_3-term.
1	Ba	−0.02	−0.16
	O	+0.24	+0.17
2	Ti	−0.10	−0.24
3	Ba	–0.12	−0.14
	O	+0.10	+0.14

Surface rumpling s (the displacement of oxygen with respect to the metal in the upper surface layer) and changes in interlayer distances Δd_{12} and Δd_{23} (1, 2 and 3 are the number of surface layers). Performed calculation results for this properties are given in Table 3. The calculations of the interlayer distances are based on the positions of relaxed metal ions. As seen from Table 5, that the BaO_3-terminated surface demonstrates the other behavior, with expansion of interlayer distance Δd12 and reduction of Δd23. In the case of Ti-terminated (111) surface shows small increase of interlayer distances Δd12 and Δd23. Calculated some values of surface rumpling and interlayer distances of surfaces in consistent with amounts from work [23].

Table 5. Calculated surface rumpling s and relative displacements Δdij between the three near-surface planes, for the BaO_3- and Ti-terminated $BaTiO_3$ (111) surfaces. Units are per cent of the bulk lattice constant

Termination	s	Δd_{12}	Δd_{23}	Termination	Δd_{12}	Δd_{23}
BaO_3-term	−0.1	0.76	−7.71	Ti-term	1.86	1.12

CONCLUSION

It is seen from the that at a graphene-layered BaO_3-terminated $BaTiO_3$ (111) surface, the band gap strongly reduced and vanished. The obtained results of research show a high sensitivity of the electronic properties of the $BaTiO_3$ (111) surface to a combination of low-dimensional systems. The main source of energetic diversity is most likely caused by charge redistribution between ions on the surface and graphene.

The calculations performed created a large amount of data for future interpretation and comparison. Designed configurations can also be used as a solid platform for OER modeling on perovskite-layered hybrid materials.

In addition, the introduction of graphene leads to the polarization of neighboring ions. The analysis of electron redistribution on the surface by introducing graphene dopants will be described in our forthcoming paper.

These studies were funded by the Ministry of Science and higher education of the Republic of Kazakhstan as part of the grant funding "Development and Research of New Multifunctional vdW Structures of 2D Films Based on Transition Metal Oxides" (IRN-AR14972694).

REFERENCES

1. Wang Q. H., Kalantar-Zadeh K., Kis A., Coleman J. N. & Strano M. S. Electronics and optoelectronics of twodimensional transition metal dichalcogenides // Nat. Nanotechnol. – 2012. – Vol.7. – P. 699–712.
2. Geim A. K. & Grigorieva I. V. A comprehensive review of stacking 2DLMs into diverse vdWHs. Van der Waals heterostructures // Nature. – 2013. – Vol. 499. – P. 419–425.
3. Andres, C.-G. [et al.] Deterministic transfer of twodimensional materials by all-dry viscoelastic stamping // 2D Mater. – 2014.– Vol. 1. – P. 011002.
4. Halim U. [et al.] A rational design of cosolvent exfoliation of layered materials by directly probing liquid–solid interaction // Nat. Commun. – 2013. – Vol. 4. – P. 2213.
5. Ye J. [et al.] Superconducting dome in a gate-tuned band insulator // Science. – 2012. – Vol. 338. – P.1193–1196.
6. Feng Q. [et al.] Growth of $MoS_{2(1-x)}$ Se_{2x} (x=0.41–1.00) monolayer alloys with controlled morphology by physical vapor deposition // ACS Nano. – 2015. – Vol. 9. – P. 7450–7455.
7. Cao Y.Unconventional superconductivity in magic-angle graphene superlattices // Nature. – 2018. – Vol. 556. – P. 43.
8. Cao Y. Correlated insulator behaviour at half-filling in magic-angle graphene superlattices // Nature. – 2018. – Vol. 556. – P. 80.
9. Petoukhoff C. E., Kosar S., Goto M., Bozkurt I., Chhowalla M., and Dani K. M. Charge transfer dynamics in conjugated polymer/MoS_2 organic/2D heterojunctions // Mol. Syst. Des. Eng. – 2019. –Vol. 4. – P. 929–938.
10. Petoukhoff C. E., Krishna M. B. M., Voiry D., Bozkurt I., Deckoff-Jones S., Chhowalla M., O'Carroll D.M., and Dani K. M. Ultrafast Charge Transfer and Enhanced Absorption in MoS2-Organic van der Waals Heterojunctions Using Plasmonic Metasurfaces // ACS Nano. – 2016. – Vol. 10. – P.9899–9908.
11. Karmakar A., Al-Mahboob A., Petoukhoff C. E., Kravchyna O., Chan N. S., Taniguchi T., Watanabe K., and Dani K. M. Dominating Interlayer Resonant Energy Transfer in Type-II 2D Heterostructure // ACS Nano. – 2022. – Vol. 16. – P. 3861–3869.
12. Gusynin V.P., Sharapov S.G., Carbotte J.P. Magnetooptical conductivity in graphene // J. Phys. Condens. Matter. – 2006. – Vol. 13. – P. 026222.
13. Hanson G.W. Dyadic Green's functions for an anisotropic, non-local model of biased graphene // IEEE Trans Antennas Propag. – 2008. – Vol. 5. – P. 747–57.
14. Gusynin V.P., Sharapov S.G., Carbotte J.P. On the universal ac optical background in graphene // New. J. Phys. – 2009. – Vol. 11. – P. 095013.
15. Dressel M., Gruner G. Electrodynamics of Solids. Cambridge University Press, Cambridge, UK. – 2002. – P. 148.
16. Sounas D.L., Calos C. Gyrotropy and nonreciprocity of graphene for microwave applications // IEEE Trans Microw Theory Tech. – 2012. – Vol. 60. – P. 901–14.
17. Acerce M., Voiry D., Chhowalla M. Metallic 1T phase MoS_2 nanosheets as supercapacitor electrode materials // Nature Nanotechnology. – 2015. – Vol. 10. – No. 4. – P. 313–318.
18. Cook J.B., Kim H., Lin T.C., Lai C., Dunn B., Tolbert S.H. Oxygen vacancies enhance pseudocapacitive charge storage properties of MoO_{3-x} // Adv. Energy Mater. – 2017. – Vol. 7. – No. 2. – P. 1601283.
19. Gigot J A., Fontana M., Serrapede M., Castellino M., Bianco S., Armandi M., Bonelli B., Pirri C.F., Tresso E., Rivolo P. Mixed 1T-2H Phase MoS_2/Reduced Graphene Oxide as Active Electrode for Enhanced Supercapacitive Performance // ACS Appl. Mater. Interfaces. – 2016. – Vol. 8. – No. 48. – P. 32842–32852.
20. Evarestov, R. A., Bandura, A. V. First-principles calculations on the four phases of $BaTiO_3$ // Journal of Computational Chemistry. – 2012. – Vol. 33(11) – P. 1123–1130. https://doi.org/10.1002/jcc.22942
21. Ghosez Ph., Gonze X., Michenaud J. -P. First-principles characterization of the four phases of barium titanate // Ferroelectrics. – 1999. Vol. 220. – Issue 1. – P. 1–15. https://doi.org/10.1080/00150199908007992
22. Uludogan M., Guarin D. P., Gomez Z. E., Cagin T., Goddard W. A. DFT Studies on Ferroelectric Ceramics and Their Alloys: $BaTiO_3$, $PbTiO_3$, $SrTiO_3$, $AgNbO_3$, $AgTaO_3$, $Pb_xBa_{1-x}TiO_3$ and $Sr_xBa_{1-x}TiO_3$ // Computer Modeling in Engineering and Sciences. – 2008. – Vol. 24. Issue 2/3. – P. 215.
23. Eglitis R. I. Ab initio hybrid DFT calculations of $BaTiO_3$, $PbTiO_3$, $SrZrO_3$ and $PbZrO_3$ (111) surfaces // Applied Surface Science. – 2015. – Vol. 358. – No. 15. –P. 556–562.

ГРАФЕН ПЛЕНКАЛАРЫМЕН КОМБИНАЦИЯЛАНҒАН РОМБОЭДРЛІК $BaTiO_3$ (111) БЕТІНІҢ AB- INITIO ЕСЕПТЕУЛЕРІ

Б. М. Сатанова[1*], Г. Ә. Қаптағай[2], А. П. Жаркымбекова[1], Ф. У. Абуова[1], А. У. Абуова[1], Р. Н. Асылбаев[3], Н. О. Қойлық[2], К. Т. Тугелбаева[2]

[1] Л.Н. Гумилев атындағы Еуразия ұлттық университеті, Астана, Қазақстан
[2] Қазақ ұлттық қыздар педагогикалық университеті, Алматы, Қазақстан
[3] Ә. Марғұлан атындағы Павлодар педагогикалық университеті, Павлодар, Казақстан

** Байланыс үшін E-mail: clever_s.balzhan@mail.ru*

ABO_3 перовскит ферроэлектриктерінің жұқа пленкалары көптеген өнеркәсіптік қолданыстар, яғни сыйымдылығы жоғары жад ұяшықтары, катализ, оптикалық толқын өткізгіштер, интегралды оптика үшін маңызды. Аталған салалар мен бұйымдар үшін $BaTiO_3$ қолдану, оның беткі құрылымының және сәйкесінше электрондық және химиялық қасиеттерінің сан алуан болуына байланысты болып табылады. $BaTiO_3$ бетінің сипаттамаларының алғашқы қағидалардан есептеулері беттік реакциялар химиясы, беткі құбылыстар және адсорбциялық беттер сияқты шешуші рөл атқаратын процестерді түсіну үшін пайдалы. Бұл зерттеу $BaTiO_3$ (111) бетінің релаксацияланған атомдық құрылымдарына қатысты теориялық есептеулерді қарастырылды.

Түйін сөздер*: гетероқұрылымдар, екі өлшемді материалдар, кіші өлшемді құрылым, өтпелі металл оксидтері, Хартри-Фок гибридті корреляциялық функциясы.*

РАСЧЕТЫ AB-INITIO РОМБОЭДРИЧЕСКОЙ ПОВЕРХНОСТИ $BaTiO_3$ (111), КОМБИНИРОВАННОЙ С ГРАФЕНОВЫМИ ПЛЕНКАМИ

Б. М. Сатанова[1*], Г. А. Каптагай[2], А. П. Жаркымбекова[1], Ф. У. Абуова[1], А. У. Абуова[1], Р. Н. Асылбаев[3], Н. О. Койлык[2], К. Т. Тугелбаева[2]

[1] Евразийский национальный университет им. Л. Н. Гумилева, Астана, Казахстан
[2] Казахский национальный женский педагогический университет, Алматы, Казахстан
[3] Павлодарский педагогический университет им. А. Маргулана, Павлодар, Казахстан

** E-mail для контактов: clever_s.balzhan@mail.ru*

Тонкие пленки перовскитных ферроэлектриков ABO_3 важны для многих промышленных применений, то есть для ячеек памяти большой емкости, катализа, оптических волноводов, интегральной оптики. Применение $BaTiO_3$ для указанных отраслей и изделий обусловлено большим разнообразием его поверхностной структуры и, соответственно, электронных и химических свойств. Расчеты характеристик поверхности $BaTiO_3$ из первых принципов полезны для понимания процессов, которые играют решающую роль, таких как химия поверхностных реакций, поверхностные явления и адсорбционные поверхности. В этом исследовании рассматривались теоретические расчеты относительно релаксированных атомных структур поверхности $BaTiO_3$ (111).

Ключевые слова: *гетероструктуры, двумерные материалы, многомерная структура, оксиды переходных металлов, гибридная корреляционная функция Хартри-Фока.*